Pump-laser-wavelength dependence of population inversion in N 2 +

Liang Xu, Chaohui Zhou, Guangyu Fan, Hongyang Cheng, Aurélien Houard, André Mysyrowicz, Vladimir Tikhonchuk, Yi Liu

Pump laser wavelength dependence of population inversion in N_2^+

Liang Xu,[1,*] Chaohui Zhou,[1] Guangyu Fan,[1] Hongyang Cheng,[1] Aurélien Houard,[2] André Mysyrowicz,[2] Vladimir T. Tikhonchuk,[3,4] and Yi Liu[1,5,†]

[1] *Shanghai Key Lab of Modern Optical System, University of Shanghai for Science and Technology, 516, Jungong Road, 200093 Shanghai, People's Republic of China*
[2] *Laboratoire d'Optique Appliquée, ENSTA Paris, CNRS, Ecole Polytechnique, Institut Polytechnique de Paris, 91762 Palaiseau, France*
[3] *University of Bordeaux-CNRS-CEA, CELIA, UMR 5107, 33405 Talence, France*
[4] *Extreme Light Infrastructure ERIC, ELI-Beamlines Facility, Za Radnicic 835, 25241 Dolní Břežany, Czech Republic*
[5] *CAS Center for Excellence in Ultra-intense Laser Science, Shanghai 201800, China*

(Dated: December 1, 2023)

We investigate the pump wavelength dependence of population inversion in nitrogen ion when nitrogen gas is irradiated by a femtosecond laser pulse in the wavelength range from ultraviolet to near-infrared. It is found that the population inversions corresponding to the transitions at 391 and 428 nm are very sensitive to the laser wavelength, with extreme values near 400 and 1000 nm. For the ultraviolet pump, the population inversions for 391 and 428 nm transitions occur at different wavelengths: a maximum inversion for the former corresponds to a minimum for the latter. This is attributed to the near-resonance single-photon transition combined with the Raman process. A significantly stronger inversion is observed for the near-infrared laser, with the maximum depending on the laser intensity, ascribed to the AC Stark effect. The Floquet theory confirms this conclusion and reveals that the three-photon transition assisted by the strong laser field leads to this enhanced population inversion. This study provides the optimal conditions for air lasing based on ionic transitions of nitrogen molecules.

I. INTRODUCTION

With intense ultrashort laser pulses, it is possible to achieve remote optical amplification from the major constituents of air: nitrogen and oxygen. The cavity-free optical amplification in air was reported in 2011 [1, 2] and has attracted much attention due to its potential application in standoff spectroscopy [3, 4], sensing [5, 6], and advanced light source [7, 8]. Forward and backward amplification has been observed in atomic oxygen and nitrogen, molecular nitrogen, and singly-ionized molecular nitrogen [9]. In contrast to cavity-free lasing in atoms and neutral molecules for which a good physical explanation is provided, the case of nitrogen ion N_2^+ is still controversial. Two theoretical models have been proposed to explain the strong amplification observed at 391 and 428 nm. The first model accounts for population inversions corresponding to the transitions between initial state $B^2\Sigma_u^+$ (designated as B) with vibrational level $\nu = 0$ and final states $X^2\Sigma_g^+$ (denoted as X) with ν =0 and 1, which is predicted by the three-state coupling model [10–12]. The second model considers a simultaneous two-photon emission/absorption process between B0 and intermediate level $A^2\Pi_u$ (denoted as A) transiting via X0 and X1 [13, 14]. Amplification of the optical field in the plasma channel is the key element of this model. Kleine *et al.* used high harmonic spectroscopy to track the strong field ionization and fragmentation dynamics of N_2^+ upon interaction with an ultrashort 800 nm laser pulse [15]. Recently, Danylo *et al.* have measured the evolution of ionic population in N_2^+ [16]. Both their observations support the second model. In addition, rotational quantum beat can suppress absorption while leaving stimulated emission intact transiently, leading to lasing without inversion [17].

Though the role of population inversion responsible for air lasing has not been fully determined yet, there is no doubt that population inversion is an important factor in favoring strong amplification of the seed pulse. Xu *et al.* predicted an increased population inversion by increasing the 800 nm-laser pulse duration [10]. The polarization-modulated ultrashort laser pulse solely or combined with the middle-infrared laser may result in a giant enhancement of N_2^+ lasing[18, 19]. Zhang *et al.* studied the dependence of population B and X as a function of pump laser wavelength [12]. However, their calculation assumed a molecular alignment with respect to the laser polarization and only dicussed the 391 nm case with a range of the pump laser wavelengths from near-infrared to middle-infrared.

In this paper, we theoretically investigate the population distribution of levels B0, X0, and X1 responsible for the lasing transitions at 391 and 428 nm as a function of pump wavelength with a broad range from ultraviolet to near-infrared and different laser intensities. We find an anti-correlation between the population inversions for 391 and 428 nm transitions in the ultraviolet region. The origin of this effect is identified by analyzing the temporal evolution of the populations during the pump pulse duration. More significant enhancements of population

* liangxu2021@usst.edu.cn
† yi.liu@usst.edu.cn

inversions for 391 and 428 nm transition are found for the laser wavelengths 900−1050 nm. This phenomenon is explained by the dominance of the three-photon transition in the strong laser field with intensity-dependent resonance due to the AC Stark shift. The results of numerical simulations are confirmed with the theoretical analysis using the Floquet approach. The paper is organized as follows. The theoretical background and the numerical method are introduced in Sec. II. Simulation results are discussed in Sec. III, and conclusions are presented in Sec. IV. Hartree atomic units are used throughout the paper unless stated otherwise.

II. THEORETICAL BACKGROUND

Two theoretical models, the density matrix and the time-dependent Schrödinger equation, are extensively used for describing a coherent light-molecule interaction system [20]. While the results of these two approaches are equivalent, the former is better suited for a multiple-electron system when considering simultaneously ionization and excitation, and is numerically more efficient. We adopt the density matrix framework here. The dynamics of N_2 ionization and N_2^+ excitation driven by an intense laser pulse is described by the Bloch equation [12, 14, 21]:

$$\frac{d\rho}{dt} = -i[H, \rho] + W. \tag{1}$$

Here ρ, H, and W represent the density matrix, system Hamiltonian, and instantaneous ionization rate, respectively. The first term on the right-hand side is the Poisson bracket, which describes the transitions between vibronic levels in N_2^+ molecule. The Hamiltonian H consists of diagonal elements $\varepsilon_{\nu\nu}$ and off-diagonal elements $H_{\nu\nu'}$, which correspond to the energies of vibrational eigenstates and the interaction between the laser field and the molecule, respectively. In addition to the ground state X, two electronic excited states are considered. The transition between X and A states, $H^{\nu\nu'}_{XA} = -\mu^{\nu\nu'}_{XA} E(t) \sin\theta$, is favored for the angle θ between the molecule axis and the direction of laser electric field E close to 90° (perpendicular orientation). The transition between X and B states, $H^{\nu\nu'}_{XB} = -\mu^{\nu\nu'}_{XB} E(t) \cos\theta$ is favored for the parallel orientation. Other electronic excited states are neglected because of their large transition energy. In total, as shown in Fig. 1, 13 vibrational levels are considered, that is, X ($\nu = 0-2$), A ($\nu = 0-4$), and B ($\nu = 0-4$). The transition dipole moments $\mu^{\nu\nu'}_{XA}$ and $\mu^{\nu\nu'}_{XB}$ and the corresponding energies are listed in Table I of Appendix A.

The instantaneous ionization rate W is represented as

$$W^{\nu\nu'}_{MM'}(\theta, t) = C^{\nu *}_{M}(\theta, t)\; C^{\nu'}_{M'}(\theta, t), \tag{2}$$

where index M denotes X, A or B electronic state, and index ν denotes the vibrational quantum number. The

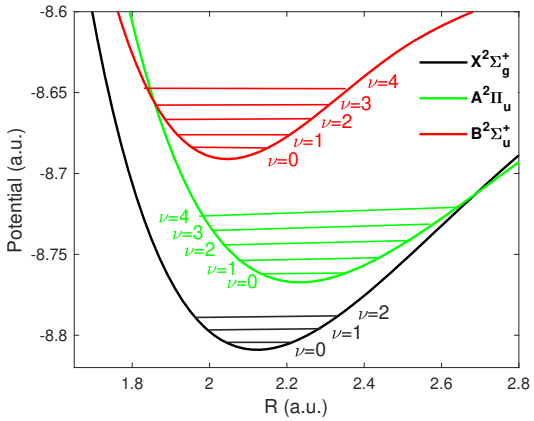

FIG. 1. (Color online) Energy diagram in N_2^+: the relevant potential energy curves for three electronic states $X^2\Sigma_g^+$ (black), $A^2\Pi_u$(green) and $B^2\Sigma_u^+$(red) as well as the corresponding nuclear vibrational states labeled by the quantum number ν.

diagonal elements of W denote the instantaneous ionization rate, which is calculated by the molecular Ammosov-Delone-Krainov theory [22–24]. The off-diagonal ones describe the coherence of ionization injection. Here we assume that the free electrons from different electronic states have the same momenta. Then the off-diagonal elements take real positive values with the coefficient C^{ν}_{M} defined by a square root of the product of ionization rate, the corresponding Franck-Condon factor, and the remaining population of neutral molecules N_2. The linearly polarized laser field is expressed by

$$E(t) = E_0 \cos(\omega t) \sin^2(\pi t/\tau), \tag{3}$$

where E_0, ω, and τ represent the laser amplitude, angular frequency, and pulse duration. Results below are presented for a typical value $\tau = 60$ fs, though similar results are obtained for the pulse duration from 40 fs to 80 fs. The laser wavelength $\lambda = 2\pi c/\omega$ is varied in the range from 300 nm to 1200 nm, and laser intensities of 1, 2, and 3×10^{14} W/cm^2 are considered.

Equation (1) is solved numerically by using the fixed-step fourth-order Runge-Kutta technique with the time step $dt = 0.02$ a.u. and the initial condition $\rho(\theta, t = 0) = 0$. The simulations are performed for the whole pulse duration $[0, \tau]$ for different angles $\theta = 0, \pi/36, \ldots, \pi$. Symmetry in the plane perpendicular to the laser polarization is assumed. The final population distribution is obtained via averaging over the polar angle,

$$\bar{P}^{\nu}_{M} = \frac{\int_0^{\pi} \rho^{\nu\nu}_{MM}(\theta, t_{\rm end}) \sin\theta \, d\theta}{\int_0^{\pi} \sin\theta \, d\theta}. \tag{4}$$

Population inversions for 391 and 428 nm lasing are calculated as $P_{391} = \bar{P}^0_B - \bar{P}^0_X$ and $P_{428} = \bar{P}^0_B - \bar{P}^1_X$, respectively. Convergence of the calculations was tested using more vibrational levels, finer angular resolution,

and smaller time steps, whereas almost identical results were obtained.

III. RESULTS AND DISCUSSION

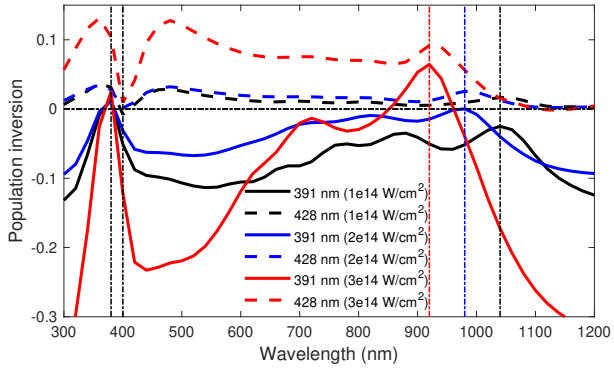

FIG. 2. (Color online) Dependence of the population inversion on the laser wavelength. Solid lines show the population inversion between B0 and X0 levels corresponding to the transition at 391 nm. Dashed lines show the inversion between B0 and X1 levels corresponding to the transition at 428 nm. Black, blue, and red lines correspond to the laser peak intensity 1, 2 and 3×10^{14} W/cm^2. The results for 1×10^{14} W/cm^2 (black lines) are multiplied by a factor 100.

Figure 2 shows the dependence of the population inversions P_{391} and P_{428} on the laser wavelength for three typical laser intensities for filaments in air. Positive populations inversion corresponding to 428 nm transition (dashed lines) are observed for all wavelengths and intensities. This is explained by the fact that level X1 is scarcely populated: Direct ionization to this level is suppressed due to the small Franck-Condon factor, and transition from the X0 level is forbidden because of the homonuclear diatomic molecule N_2^+. By contrast, the population inversion for emission at 391 nm (solid lines) strongly depends on the laser wavelength, showing no population inversion in the range from 400 nm to 700 nm and maximums in the near-infrared and ultraviolet regions. Specifically, in the near-infrared band, as the laser intensity increases from 1 to 3×10^{14} W/cm^2, the wavelength for maximum population inversion appears around 1040 nm and shifts to 920 nm. Vertical dash-dot lines mark the positions of maximums.

As shown in Fig. 2, population inversion for 391 nm emission is already created at the laser intensity 2×10^{14} W/cm^2 (black solid line). This intensity value is smaller than that shown in previous reports [2, 10, 11, 24, 25], though the ionization probability is low at this intensity. The wavelengths for maximum population inversion for 391 and 428 nm transitions occur at the same wavelength in the infrared region. As shown below, this can be ascribed to the population increase in level B0 since this level is common for both transitions. By contrast, there

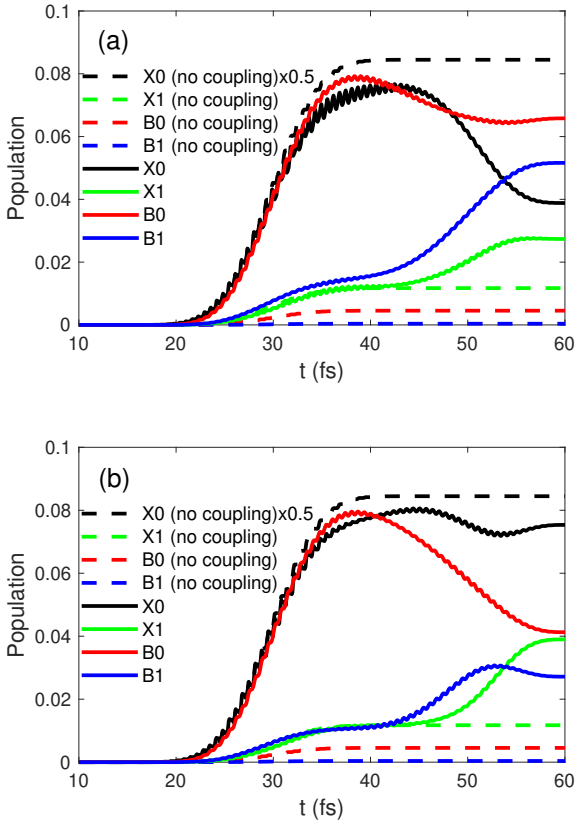

FIG. 3. (Color online) The time dependence of populations in levels X0 (black), X1 (green), B0 (red) and B1 (blue) for $\theta = 45°$. Laser peak intensity is 2×10^{14} W/cm^2; the wavelength is 380 nm (a) and 400 nm (b). The dashed lines show the calculation where only ionization is included. The result for X0 (black dashed line) is multiplied by a factor 0.5.

is an anti-correlation of population inversions in the ultraviolet region. The minimum at about 400 nm for the emission at 428 nm coincides nearly with the maximum for the emission at 391 nm. This is indicated by two left vertical dash-dot lines in Fig. 2. These observations highlight the significant difference in the excitation dynamics between the infrared and ultraviolet domains.

To better understand the mechanisms of population inversion in the ultraviolet region, we consider the evolution of relevant populations at the typical intensity 2×10^{14} W/cm^2. The coupling between X and A states is very weak in this range because of a large detuning between photon energy and energy of transition. Nevertheless, the direct ionization for molecules aligned in the plane perpendicular to the laser polarization, $\theta = 90°$, should not be ignored. Hence, we select an intermediate angle $\theta = 45°$ and trace the time dependence of populations in levels X and B for two laser wavelengths of 380 nm and 400 nm, as shown in Fig. 3.

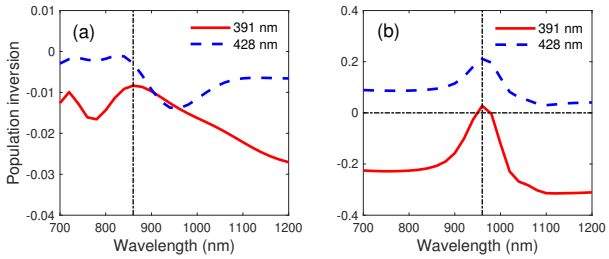

FIG. 4. (Color online) Dependence of population inversion for the transitions at 391 nm (red solid lines) and 428 nm (blue dashed lines) on the laser wavelength for the molecule alignment angle $\theta = 90^\circ$ (a) and $\theta = 0^\circ$ (b). Laser intensity is $I = 2 \times 10^{14}$ W/cm^2.

The results considering only ionization processes are also shown for comparison with dashed lines. The dominant process is the ionization of neutral molecules to the ground level X0 in N_2^+, while excitation to the levels B0 and B1 is due to the single-photon transitions. A notable fraction of ions in panels (a) and (b) are quickly transferred to the B0 level before 40 fs. However, as shown in panel (a), level B1 is populated directly from X0 in the the second half of the pulse and partially decays into X1 via the Stokes Raman process. Conversely, for the laser wavelength at 400 nm shown in panel (b), population of level B0 is partially transferred to X1 and then returns to B1 via the anti-Stokes Raman effect, which is favored by the resonance interaction of the X1-B1 transition channel with a 400 nm photon. These coherent processes maximize the population in level X1 and minimize that in B0. They are at the origin of the minimum population inversion for 428 nm emission for the laser wavelength of about 400 nm. To summarize briefly, the near-resonance single-photon transmission combined with the Raman process are responsible for the peak of 391 nm inversion at 380 nm and the dip of 428 nm inversion at 400 nm. We notice that a similar mechanism of population inversion was discussed in Ref. [26].

In contrast to the ultraviolet case, the enhanced peaks of population inversion in the near-infrared range show an intensity dependence, which suggests an importance of the intensity-modulated AC Stark effect. To reveal the underlying mechanism, we consider separately two representative molecular alignments, as demonstrated in Fig. 4. In the case of transverse orientation shown in panel (a), ionization to the B level dominates and the popluation in B0 is very small because of its larger ionization energy. Although a fraction of molecules is transferred from X0 to the vibrational levels $\nu = 0, 1, 2$ in A, this single-photon transition is insufficient to create inversions for 391 nm and 428 nm emissions. As shown in Fig. 4(b), the situation is quite different for the molecules aligned parallel to the laser field. Although the transition from X0 to A state is suppressed, molecules are transferred efficiently from X0 to B0 level, thus creating population inversions. This process of the direct X0-B0 transition is different from the transfer through the intermediate A state studied in [10, 11, 14, 25, 27].

The direct transfer X0-B0 in the case of parallel orientation of molecule, shown in Fig. 4(b), is a three-photon process. Indeed, according to the transition rules, only odd-photon processes between X and B states are allowed. The field-free energy gap between X0 and B0 levels is 0.1175 a.u. (3.2 eV), and the single-, three-, and five-photon transitions correspond to the laser wavelengths 391 nm, 1173 nm, and 1955 nm. The single-photon transition is already considered: it corresponds to the ultraviolet region. The three-photon resonant wavelength of 1173 nm is quite different from the maximum population inversion observed at the laser wavelength of 980 nm. The AC Stark effect can explain this blue shift of the three-photon resonance phenomenologically.

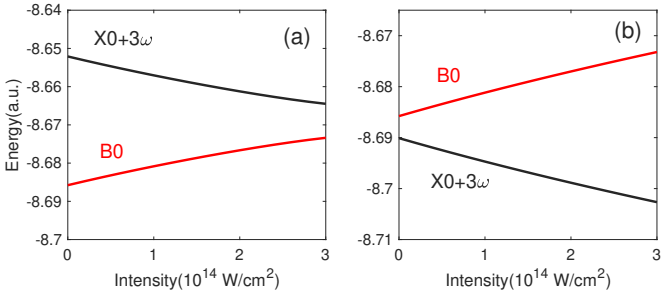

FIG. 5. (Color online) Dependence of the shifts of X0 and B0 energy levels on the laser intensity for the laser wavelength 900 nm (a) and 1200 nm (b). Up to five-photon transitions are considered in the Floquet matrix.

Molecules in a strong laser field are exposed to the AC Stark effect. While it is accounted for in the density matrix formalism Eq. (1), it would be interesting to evaluate it qualitatively. The Stark shift can be estimated theoretically using the Floquet theory [28], which considers the interaction of a quantum system with an external AC field at the main frequency and its harmonics. The structure of the Floquet matrix is shown in Appendix B. It contains diagonal terms describing quantum levels and nonzero off-diagonal terms accounting for the coupling to the external field and its harmonics. The laser-dressed eigenstates are obtained by diagonalizing the Floquet matrix. We consider a laser field with a constant amplitude and account for the transitions including up to five photons.

The dependence of energy shift of X0 and B0 levels on laser intensity is presented in Fig. 5 for the representative laser wavelengths of 900 and 1200 nm. Similarly to the case of the DC Stark effect, the ground level shifts downward, and the excited level moves upward; that is, the gap increases with the laser intensity. The three-photon interaction makes the dominant contribution. In the case of a laser wavelength of 900 nm shown in Fig. 5(a), the energy of three photons is larger than the free-field energy gap. Therefore, the transition approaches the resonance

as the laser intensity increases. By contrast, in the case of 1200 nm, the energy of three photons is smaller than the free-field gap. Therefore, as the laser intensity rises, the mismatch increases and the system moves out of resonance more and more, as presented in Fig. 5(b).

Calculations performed for other laser wavelengths from 900 nm to 1200 nm confirm that the energy gap always increases with the laser intensity for three-photon process. This is consistent with a monotonous blue shift of the wavelength for maximum population inversion with intensity shown in Fig. 2. This analysis confirms that among two competing channels of population inversion: the parallel three-photon transition between X0 and B0 levels, and the perpendicular single-photon two-step transition through the A states, the former channel dominates. As a matter of fact, the dynamic three-photon process is very complicated in interwoven time and frequency domains, where the interactions between all vibrational states via light fields contribute to the multi-photon transition together. Thus, the Floquet theory can only give a rough picture here.

IV. CONCLUSIONS

We studied the dependence of N_2 molecule ionization and ion N_2^+ excitation on the wavelength and intensity of a femtosecond laser pulse. The density matrix equations based on the coherent ionization-coupling model are solved numerically, assuming an isotropic orientation of the molecules with respect to the laser polarization. A combined effect of ionization and excitation results in the population inversion between B0 and X0 and X1 states in two particular spectral domains of near 400 and 980 nm, corresponding to the resonance single-photon and three-photon transitions between the ground state X0 and excited state B0.

A narrow range of pump laser wavelength for maximum population inversion in the ultraviolet domain is attributed to the near-resonance single-photon excitation accompanied by the Raman scattering. An anti-correlation between the population inversions corresponding to B0-X0 and B0-X1 transitions is related to the fact that level X1 is populated from B0 during the laser pulse.

By contrast, a broad peak around 1000 nm is strongly blue-shifted from the expected position at 1173 nm due to the three-photon AC Stark effect. The direct calculation of the population inversion using the density matrix formalism is qualitatively confirmed by the Floquet method. Similarly to the DC Stark effect, the energy gap between the ground and excited levels always increases from the free-field position for three-photon process. The three-photon transition dominates and leads to an efficient population transfer to B0 level. A similar effect is expected in the wavelength domain of $1500-1800$ nm due to the five-photon process. However, simulations show that the probability of this process is much lower, and no population inversion is expected. A similar process of population inversion should also occur for the oxygen atom.

ACKNOWLEDGMENTS

This work was supported by the National Natural Science Foundation of China (12204308, 12034013, 12374318) and the Shanghai Science and Technology Commission (Grants No. 22ZR1444100).

Appendix A: Relevant molecular parameters

TABLE I. The vibration-dependent energy gap $\Delta\mathcal{E}_{\nu\nu'}$ and transition dipole moment $\mu_{\nu\nu'}$ between the N_2^+ electronic states $X^2\Sigma_g^+$ and $A^2\Pi_u$. The magnitude of dipole moments is calculated from the Einstein coefficients A_{ab} provided in Ref. [29], and the sign is calculated numerically by the diagonalization for three potential curves [24].*

$N_2^+(\nu-\nu')$	$\Delta\mathcal{E}_{\nu\nu'}$ (a.u.)	$\mu_{\nu\nu'}$ (a.u.)
X(0)-A(0)	0.04145	0.1764
X(0)-A(1)	0.05006	0.1488
X(0)-A(2)	0.05854	0.0977
X(0)-A(3)	0.06687	0.0570
X(0)-A(4)	0.07507	0.0313
X(1)-A(0)	0.03145	-0.1505
X(1)-A(1)	0.04006	0.0466
X(1)-A(2)	0.04854	0.1241
X(1)-A(3)	0.05688	0.1182
X(1)-A(4)	0.06507	0.0862
X(2)-A(0)	0.02160	0.0808
X(2)-A(1)	0.03021	-0.1421
X(2)-A(2)	0.03869	-0.0350
X(2)-A(3)	0.04703	0.07446
X(2)-A(4)	0.05523	0.1107
X(0)-B(0)	0.11752	0.5783
X(0)-B(1)	0.12842	0.3596
X(0)-B(2)	0.13911	0.1258
X(0)-B(3)	0.14946	-0.0235
X(0)-B(4)	0.15959	0.0004
X(1)-B(0)	0.10754	0.3769
X(1)-B(1)	0.11843	-0.3412
X(1)-B(2)	0.12911	-0.4175
X(1)-B(3)	0.13949	0.1901
X(1)-B(4)	0.14956	0.1217
X(2)-B(0)	0.09769	0.2003
X(2)-B(1)	0.10858	-0.3985
X(2)-B(2)	0.11926	0.1627
X(2)-B(3)	0.12965	-0.4207
X(2)-B(4)	0.13974	-0.2352

Appendix B: Floquet matrix

The Floquet matrix is calculated for X and B levels from the time-dependent Schrödinger equation, assuming laser filed of a constant amplitude and frequency ω. It utilizes the time periodicity of the system Hamiltonian, and considers only the information in the frequency domain for X and B states. $\mathcal{E}_{X/B}$ denotes the energy of vibrational level in the electronic state X or B, and $\Omega = -\mu_{XB}^{\nu\nu'} E_0 \cos\theta$ is the Rabi frequency. Transitions with up to five photons are considered.

The matrix of the Floquet Hamiltonian has the following form [28]:

$$\begin{pmatrix}
\cdot & \cdot & \cdot & \cdot & \cdot & \cdot & \cdot & \cdot & \cdot & \cdot \\
\cdot & \mathcal{E}_B - 2\omega & \Omega/2 & 0 & 0 & 0 & 0 & 0 & 0 & \cdot \\
\cdot & \Omega^*/2 & \mathcal{E}_X - \omega & 0 & 0 & \Omega/2 & 0 & 0 & 0 & \cdot \\
\cdot & 0 & 0 & \mathcal{E}_B - \omega & \Omega^*/2 & 0 & 0 & 0 & 0 & \cdot \\
\cdot & 0 & 0 & \Omega^*/2 & \mathcal{E}_X & 0 & 0 & \Omega/2 & 0 & \cdot \\
\cdot & 0 & \Omega^*/2 & 0 & 0 & \mathcal{E}_B & \Omega/2 & 0 & 0 & \cdot \\
\cdot & 0 & 0 & 0 & 0 & \Omega^*/2 & \mathcal{E}_X + \omega & 0 & 0 & \cdot \\
\cdot & 0 & 0 & 0 & \Omega^*/2 & 0 & 0 & \mathcal{E}_B + \omega & \Omega/2 & \cdot \\
\cdot & 0 & 0 & 0 & 0 & 0 & 0 & \Omega^*/2 & \mathcal{E}_X + 2\omega & \cdot \\
\cdot & \cdot & \cdot & \cdot & \cdot & \cdot & \cdot & \cdot & \cdot & \cdot
\end{pmatrix}$$

[1] A. Dogariu, J. B. Michael, M. O. Scully, *et al.*, High-gain backward lasing in air, Science **331**, 442 (2011).

[2] J. Yao, B. Zeng, H. Xu, G. Li, W. Chu, J. Ni, H. Zhang, S. L. Chin, Y. Cheng, and Z. Xu, High-brightness switchable multiwavelength remote laser in air, Phys. Rev. A **84**, 051802(R) (2011).

[3] P. R. Hemmer, R. B. Miles, P. Polynkin, T. Siebert, A. V. Sokolov, P. Sprangle, and M. O. Scully, Standoff spectroscopy via remote generation of a backward- propagating laser beam, Proc. Natl. Acad. Sci. U.S.A. **108**, 3130 (2011).

[4] X. Zhang, Q. Lu, H. C. Mei, S. Y. Qin, Y. Gao, A. Houard, V. T. Tikhonchuk, A. Mysyrowicz, L. Xu, and Y. Liu, Standoff detection of an electric field by bidirectional nitrogen lasing, Phys. Rev. A **108**, 033513 (2023).

[5] J. Ni, W. Chu, H. Zhang, B. Zeng, J. Yao, L. Qiao, G. Li, C. Jing, H. Xie, H. Xu, Y. Cheng, and Z. Xu, Impulsive rotational Raman scattering of N_2 by a remote "air laser" in femtosecond laser filamen, Opt. Lett. **39**, 2250 (2014).

[6] Zhihao Zhang, Fangbo Zhang, Bo Xu, Hongqiang Xie, Botao Fu, Xu Lu, Ning Zhang, Shupeng Yu, Jinping Yao, Ya Cheng, Zhizhan Xu, High-sensitivity gas detection with air-lasing-assisted coherent raman spectroscopy, Ultrafast Sci. **2022**, 9761458 (2022).

[7] H. Lei, J. Yao, J. Zhao, H. Xie, F. Zhang, H. Zhang, N. Zhang, G. Li, Q. Zhang, X. Wang, Y. Yang, L. Yuan, Y. Cheng, and Z. Zhao, Ultraviolet supercontinuum generation driven by ionic coherence in a strong laser field, Nat. Commun. **13**, 4080 (2022).

[8] Y. Wan, Z. Liu, J. Yao, B. Xu, J. Chen, F. Zhang, Z. Zhang, L. Qiao, and Y. Cheng, A spectrally bright wavelength-switchable vacuum ultraviolet source driven by quantum coherence in strong-field-ionized molecules, New J. Phys. **23**, 023005 (2021).

[9] L. Yuan, Y. Liu, J. Yao, and Y. Cheng, Recent advances in air lasing: A perspective from quantum coherence, Adv. Quantum Technol. **2**, 1900080 (2019).

[10] H. Xu, E. Lötstedt, A. Iwasaki, and K. Yamanouchi, Sub-10-fs population inversion in N_2^+ in air lasing through multiple state coupling, Nat. Commun. **6**, 8347 (2015).

[11] J. Yao, S. Jiang, W. Chu, B. Zeng, C. Wu, R. Lu, Z. Li, H. Xie, G. Li, C. Yu, Z. Wang, H. Jiang, Q. Gong, and Y. Cheng, Population redistribution among multiple electronic states of molecular nitrogen ions in strong laser fields, Phys. Rev. Lett. **116**, 143007 (2016).

[12] Q. Zhang, H. Xie, G. Li, X. Wang, H. Lei, J. Zhao, Z. Chen, J. Yao, Y. Cheng, and Z. Zhao, Sub-cycle coherent control of ionic dynamics via transient ionization injection, Commun. Phys. **3**, 50 (2020).

[13] A. Mysyrowicz, R. Danylo, A. Houard, V. Tikhonchuk, X. Zhang, Z. Fan, Q. Liang, S. Zhuang, L. Yuan, and Y. Liu, Lasing without population inversion in N_2^+, APL Photonics **4**, 110807 (2019).

[14] V. T. Tikhonchuk, Y. Liu, R. Danylo, A. Houard, and A. Mysyrowicz, Theory of femtosecond strong field ion excitation and subsequent lasing in N_2^+, New J. Phys. **23**, 023035 (2021).

[15] C. Kleine, M.-O. Winghart, Z.-Y. Zhang, M. Richter, M. Ekimova, S. Eckert, M. J. J. Vrakking, E. T. J. Nibbering, A. Rouzée, and E. R. Grant, Electronic state population dynamics upon ultrafast strong field ionization and fragmentation of molecular nitrogen, Phys. Rev. Lett. **129**, 123002 (2022).

[16] R. Danylo, G. Lambert, M. Redkin, A. Houard, X. Zhang, Y. Liu, L. Xu, A. Couairon, V. Tikhonchuk, and A. Mysyrowicz, Evolution of the populations of ionic electronic levels during lasing of molecular nitrogen at 391.4 nm: evidence of a two photon amplification process in a V scheme arrangement, (To be published).

[17] M. Richter, M. Lytova, F. Morales, S. Haessler, O. Smirnova, M. Spanner, and M. Ivanov, Rotational quantum beat lasing without inversion, Optica **7**, 586 (2020).

[18] H. Li, M. Hou, H. Zang, Y. Fu, E. Lötstedt, T. Ando, A. Iwasaki, K. Yamanouchi, and H. Xu, Significant enhancement of N_2^+ lasing by polarization-modulated ultrashort laser pulse, Phys. Rev. Lett. **122**, 013202 (2019).

[19] Hanxiao Li, Erik Lötstedt, Helong Li, Yan Zhou, Nana Dong, Lunhua Deng, Peifen Lu, Toshiaki Ando, Atsushi Iwasaki, Yao Fu, Siqi Wang, Jian Wu, Kaoru Yamanouchi, and Huailiang Xu, Giant enhancement of air lasing by complete population inversion in N_2^+, Phys. Rev. Lett. **125**, 053201 (2020).

[20] M. O. Scully and M. S. Zubairy, *Quantum Optics* (Cambridge University Press, 1997).

[21] J. Chen, J. Yao, H. Zhang, Z. Liu, B. Xu, W. Chu, L. Qiao, Z. Wang, J. Fatome, O. Faucher, C. Wu, and Y. Cheng, Electronic-coherence-mediated molecular nitrogen-ion lasing in a strong laser field, Phys. Rev. A **100**, 031402(R) (2019).

[22] X. M. Tong, Z. X. Zhao and C. D. Lin, Theory of molecular tunneling ionization. Phys. Rev. A **66**, 033402 (2002).

[23] Song-Feng Zhao, Cheng Jin, Anh-Thu Le, T. F. Jiang, and C. D. Lin, Determination of structure parameters in strong-field tunneling ionization theory of molecules, Phys. Rev. A **81**, 033423 (2010).

[24] L. Xu, Q. Lu, V. T. Tikhonchuk, B. Zhou, R. Yang, Q. Liang, F. He, R. Danylo, A. Houard, A. Mysyrowicz, and Y. Liu, Quantum and quasi-classical effects in the strong field ionization and subsequent excitation of nitrogen molecules, Opt. Express **30**, 38481 (2022).

[25] Vladimir T. Tikhonchuk, Yi Liu, Rostyslav Danylo, Aurélien Houard, and André Mysyrowicz, Modeling of the processes of ionization and excitation of nitrogen molecules by short and intense laser pulses, Phys. Rev. A **104**, 063116 (2021).

[26] Siqi Wang, Erik Lotstedt, Jincheng Cao, Yao Fu, Hongwei Zang, Helong Li, Toshiaki Ando, Atsushi Iwasaki, Kaoru Yamanouchi, and Huailiang Xu, Population inversion in N_2^+ by vibrationally mediated Rabi oscillation at 400 nm,Phys. Rev. A **104**, 032823 (2021).

[27] Q. Lu, X. Zhang, S. López, H. Mei, L. Xu, Q. Liang, A. Houard, V. Tikhonchuk, A. Mysyrowicz, E. Oliva, and Y. Liu, Spectral splitting of the lasing emission of nitrogen ions pumped by 800-nm femtosecond laser pulses, Opt. Lett. **48**, 664 (2023).

[28] R. V. Krems, *Molecules in Electromagnetic Fields* (John Wiley & Sons, 2019).

[29] F. R. Gilmore, R. R. Laher, and P. J. Espy, Franck–Condon factors, r-Centroids, Electronic Transition moments, and Einstein coefficients for many nitrogen and oxygen band system, J. Phys. Chem. Ref. Data **21**, 1005 (1992).